Fabrication of ultrafine nanostructures with single-nanometre precision in a high-resolution transmission electron microscope

2007 Nanotechnology 18 155303

IOP PUBLISHING NANOTECHNOLOGY
Nanotechnology **18** (2007) 155303 (6pp) doi:10.1088/0957-4484/18/15/155303

Fabrication of ultrafine nanostructures with single-nanometre precision in a high-resolution transmission electron microscope

Jingmin Zhang, Liping You, Hengqiang Ye and Dapeng Yu

Electron Microscopy Laboratory, School of Physics, Peking University, Beijing 100871, People's Republic of China

E-mail: yudp@pku.edu.cn

Received 21 December 2006, in final form 17 February 2007
Published 9 March 2007
Online at stacks.iop.org/Nano/18/155303

Abstract
Highly ordered ultrafine nanostructures (feature size <10 nm) have been successfully fabricated with single-nanometre precision using a convergent electron beam (CEB) in a high-resolution transmission electron microscope (HRTEM). This approach can be widely applied to inorganic solid-state materials including insulators, semiconductors and metals. The feature size can be precisely controlled by the probe size and the irradiation time. The formation mechanism of nanostructures fabricated by CEB has been discussed in terms of knock-on damage and the beam heating effect. On the basis of the experimental results of electron energy-loss spectroscopy (EELS), finite element thermal analysis reveals that the heating effect of the high-energy electron beam is negligible in inorganic solid-state materials, and the sculpting of nanostructures is predominated by the knock-on damage or ionization of high-energy electrons.

1. Introduction

Highly ordered nanopore arrays with a feature size >20 nm have been fabricated by a radio-frequency magnetron sputtering method [1] and a chemical etching method [2]. However, these methods are confined to certain materials and it is difficult to reduce the nanopore size to several nanometres, which is critical to many techniques for manipulating single particles, such as sequencing single bio-molecules [3–9], detection of single particles [10], quantum fluidics [11] and atomic wave diffraction [12–14]. Progress has been made recently in the fabrication of a single nanopore with a feature size of <10 nm via shrinking a large pore by exposure to an ion or electron beam [15, 16]. In the so-called 'ion-beam sculpting' method [15], a pore of several tens of nanometres in diameter is initially created by reactive ion etching or by a focused ion beam, and then the pore is shrunk to a nanopore by argon beam exposure. In the electron beam method [16], a 20 nm pore is first opened in a silicon membrane by electron-beam lithography and anisotropic etching, and then it is reduced to a single nanometre by exposing it to a broadening electron beam after the membrane is thermally oxidized. The above methods have clear contributions to ultrafine nanofabrication, but it is difficult to use them to fabricate more complicated ultrafine nanostructures, such as nanopore arrays and nanogratings. In this paper, we report a simple approach to fabricate highly ordered ultrafine nanostructures at will in a high-resolution transmission electron microscope. This approach can be applied not only to insulators but also to semiconductors and metals.

2. Approaches and experimental details

In the convergent beam electron diffraction (CBED) analysis, we found that the penetration ability of a finely focused electron beam with high current density and high accelerating energy goes beyond our imagination. When the electron beam is finely focused into a nanoprobe, the total beam current is concentrated in a nanoscale region where the current density is very strong. An ultrafine nanopore is formed in several

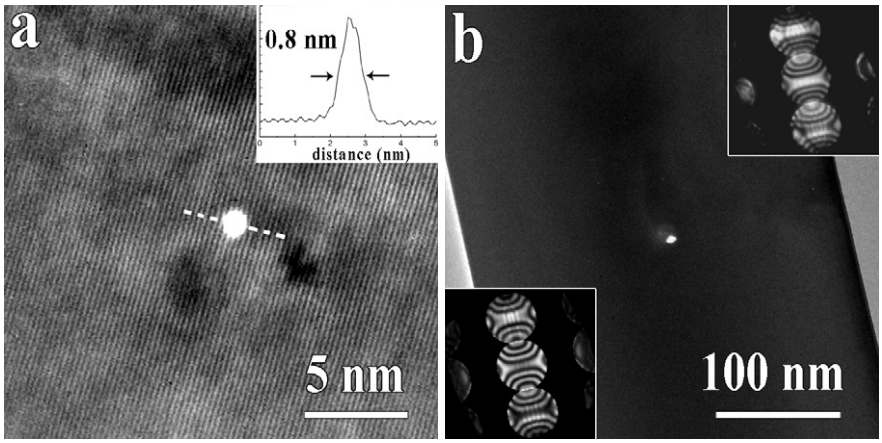

Figure 1. (a) Sub-nanometre pore drilled in a 40 nm diameter ZnO nanowire. The intensity profile at the dashed line is given in the inset. (b) Nanopore (about 5 nm in diameter) drilled in a 0.3 μm thick ZnO nanorod, the thickness was determined from a comparison of the experimental and simulated CBED patterns, as shown in the insets (upper, experimental; lower, simulated).

tens of seconds due to the greatly enhanced electron-beam irradiation, which makes the rapid fabrication of complicated ultrafine nanostructures and the penetration of thick materials feasible. The apparatus used in this work is a high-resolution transmission electron microscope (TEM, Tecnai F30) with a field emission gun operating at a 300 kV accelerating voltage. The convergent electron beam has a diameter of about 1 nm with a convergence semi-angle of ∼4 mrad. The current density is estimated to be around 3×10^4 A cm^{-2}.

In order to show the precise control of the CEB, a sub-nanometre pore was drilled in a 40 nm diameter ZnO nanowire with an irradiation time of 10 s, as shown in figure 1(a). The ZnO nanowires were synthesized via thermal evaporation of zinc powder [17]. The full width at half maximum measured from the intensity profile of the nanopore was ∼0.8 nm. Such a small pore covers 3–4 (001) lattice plane spacings only, and is comparable to the molecule size and the smallest nanotunnels in natural zeolites. Moreover, we demonstrated that the CEB has a very powerful ability to penetrate thick materials. In figure 1(b), a nanopore of ∼5 nm in diameter was drilled through a sub-micron ZnO rod of 0.3 μm in thickness within 15 min. The thickness was determined from a comparison of the experimental and simulated convergent beam electron diffraction patterns, as shown in the insets. The diameter/depth aspect ratio is >50, which is much higher than that achieved via today's conventional nanofabrication techniques.

It is found that the probe size of the CEB has a crucial effect on the size of the sculpted structures, which is manifested by ten serial nanopores drilled using different probe sizes in a ZnO membrane (figure 2(a)), and the irradiation time remains as 100 s per pore. The probe size decreases from left to right. It is clear that the smaller the probe size, the smaller the diameter of the nanopore. Similarly, the influence of the irradiation time of the CEB on feature size was revealed by the sculpture of a series of nanopores using the same probe size on a nickel membrane at different irradiation times from 100 to 20 s. The longer the irradiation time, the larger the nanopore fabricated, as shown in figure 2(b). Figure 2(c) shows that the nanopore diameter increases almost linearly with the irradiation time.

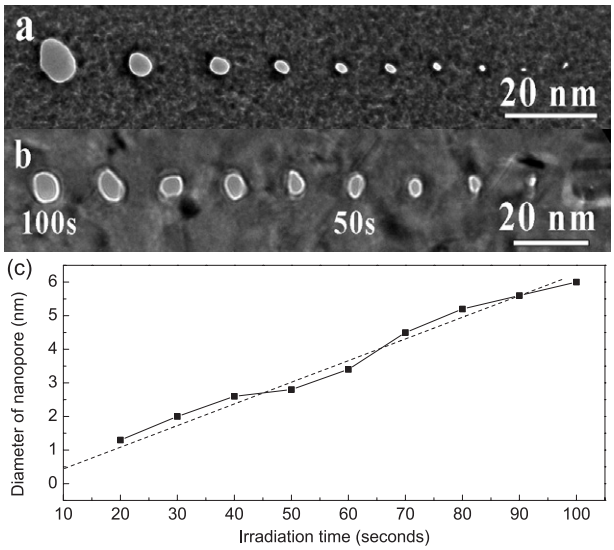

Figure 2. (a) Probe size effect on the nanopore diameter in a ZnO membrane. The probe size decreases from left to right. ((b), (c)) Irradiation time effect on the nanopore diameter in a nickel membrane.

Therefore, the feature size of ultrafine nanostructures can be precisely controlled by the probe size and the irradiation time.

Complicated ultrafine nanostructures can be fabricated using the approach described above. Nanopores composing the letters 'DNA' were sculpted in a ZnO nanowire (figure 3(a)). The nanopore diameter is around 3 nm, corresponding to an irradiation time of 20 s per pore. In figure 3(b), the high-resolution TEM image reveals that the nanopores have atomic-clear edges surrounded by perfect lattice fringes. The atomic-sharp edges indicate that the nanopores fabricated in this work are mechanically robust, in contrast to the amorphous edge of those in previous studies. It is noted that the atomic lattices between nanopores remain perfect even when the spacing between two nanopores decreases to ∼1.5 nm. This result indicates that the proximity effect is negligible in our approach.

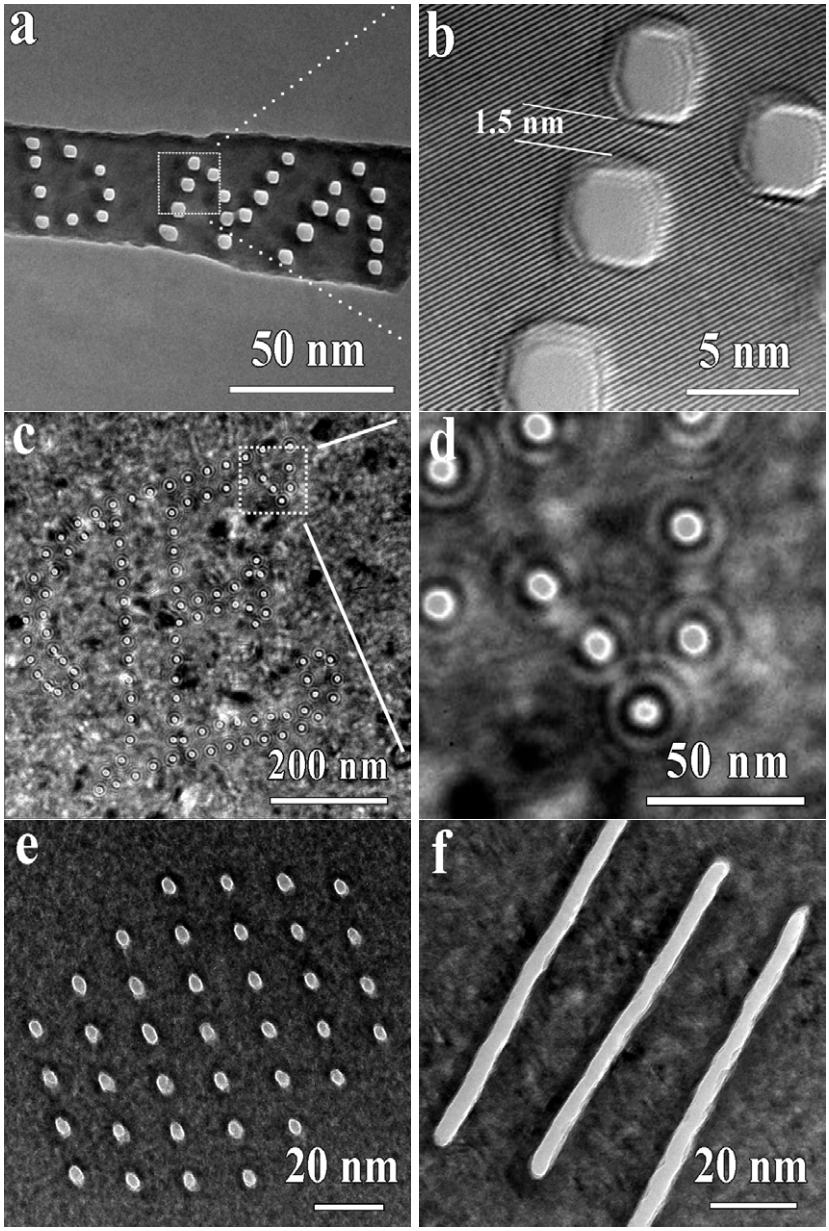

Figure 3. (a) Low-magnification TEM image of 'DNA' nanopores in a ZnO nanowire. (b) High-resolution TEM image at the top-left corner of the letter 'N'. (c) Letter 'E' sculpted in a 30 nm thick nickel membrane, (d) magnified TEM image of (c) with Fresnel diffraction fringes. (e) Nanopore array and (f) nanograting sculpted in a 100 nm thick ZnO membrane.

Highly ordered ultrafine nanostructures, such as nanopore arrays and nanogratings, can be automatically sculpted at will with single-nanometre precision using a control program. A program has been coded to control the scan and the irradiation time of the CEB automatically, which greatly increases the efficiency to sculpt different ultrafine nanostructures. We demonstrate a letter 'E', consisting of 110 nanopores, which was written with a ∼5 nm probe size and an irradiation time of 20 s per nanopore in a 30 nm thick nickel membrane (figure 3(c)). The nanopore diameter, ∼6 nm, is confirmed by the magnified TEM image in figure 3(d). Fresnel diffraction fringes obviously confirm the penetration of nanopores. All of the nanopores are precisely in their positions as designed. In a similar way, a nanopore array was demonstrated in a 100 nm thick ZnO membrane, as shown in figure 3(e). The ZnO membranes used were synthesized using the electrodeposition method [18]. If the CEB is continuously moved, a nanograting can be fabricated, as shown in figure 3(f). This indicates that the CEB can also be used as a fine cutting tool to reshape nanostructures with single-nanometre precision. Three-dimensional nanopatterns may also be fabricated by tilting the specimen.

Extended studies revealed that our approach is not only effective for oxide materials, but is also applicable to a diverse variety of solid-state materials including insulators, semiconductors and metals. To demonstrate the applicability of this approach, nanopores have been fabricated in single crystalline Si membrane, Si_3N_4 nanowire, α-Al_2O_3 membrane,

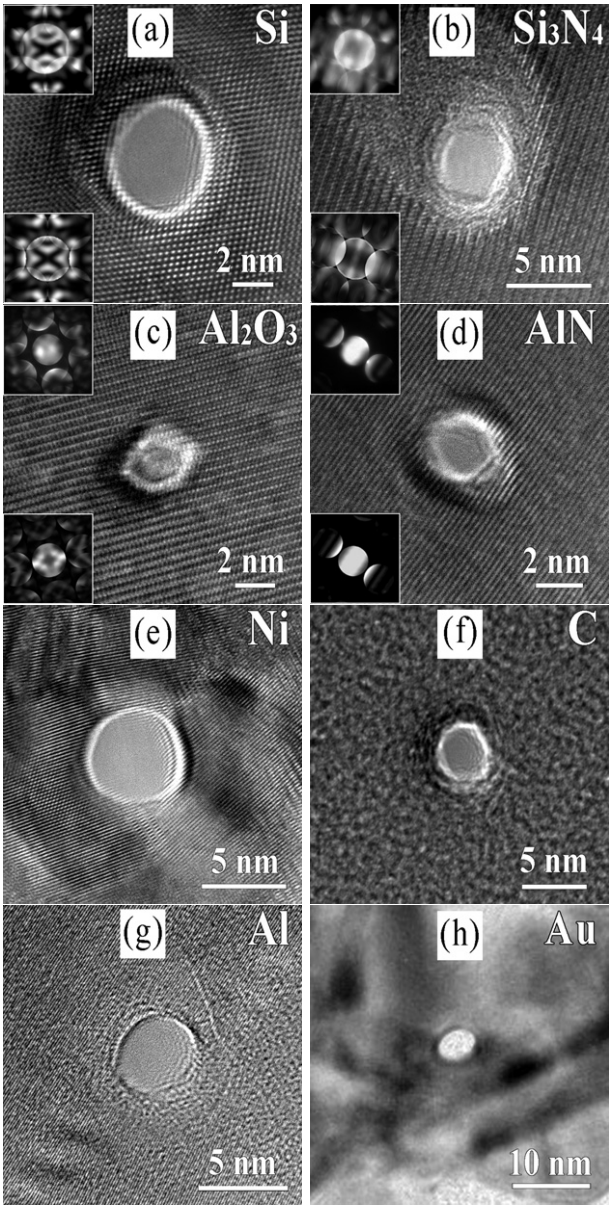

Figure 4. Nanopore sculpted in (a) 160 nm thick Si[110] membrane, (b) 100 nm thick Si_3N_4[100] nanowire, (c) 95 nm thick α-Al_2O_3[210] membrane, (d) 80 nm thick AlN[141] nanorod, (e) 30 nm thick polycrystalline nickel film, (f) 15 nm thick amorphous carbon film, (g) 30 nm thick polycrystalline aluminium film, and (h) 30 nm thick polycrystalline gold film. In (a)–(d), the thickness and zone axis were determined from a comparison of the experimental (upper) and simulated (lower) CBED patterns, as shown in the insets.

AlN nanorod, Ni film, amorphous carbon film, Al film, and gold film, as shown in figure 4. The silicon and α-Al_2O_3 membranes were prepared by the standard preparation method for TEM thin foils by the ion-milling technique. Si_3N_4 nanowire and AlN nanorod were grown by the chemical vapour deposition method [19, 20]. Nickel, carbon, aluminium, and gold films were deposited on single crystalline NaCl substrates by the electron beam evaporation method. The NaCl substrate was dissolved in distilled water, and the floating films were transferred onto TEM grids. The thickness as well as zone axis was determined from the CBED patterns, as shown in the insets. Analysis of the intensity profile of the TEM images shows that the diameters of the nanopores in figure 4 are in the range of 2–5 nm. The asymmetric bright–dark contrast surrounding the nanopore indicates the presence of beam-damage-induced strains.

3. Discussion

The beam-induced damage primarily involves the heating effect, ionization and knock-on damage of fast electrons due to the moderate energy (300 keV) of the electron beam used in this work [21]. In the experiments we found that sculpting aluminium and nickel films was much easier than that of gold films. This indicates that the lighter the metal atoms in the film, the easier it is to drill pores in it. The sculpture of metals suffers mainly knock-on damage due to their excellent thermal conductivities [21, 22]. For the semiconductors and insulating materials, the beam heating effect might also work due to their low thermal conductivities. However, the direct temperature measurement of a nanoscale area in TEM is rather difficult, and the relevant studies have rarely been reported. The beam heating effect in TEM is unclear and is still disputed. In this work, finite element thermal analysis has been attempted to qualitatively estimate the heating effect of the CEB in a ZnO membrane, even though the finite element calculations are based on a linear continuum theory of heat transport. We simply assume that the electron energy loss caused by the inelastic interactions totally contributes to the beam heating effect. This assumption slightly overestimates the result because the energy loss caused by other electron beam interactions (such as core–shell excitation, ionization and knock-on etc) is regarded as the contribution to the heating effect, and the thermal radiation has not been taken into account. Although this assumption is not rigorous, it should be sufficient for qualitative analysis.

According to the above assumption, the EELS spectrum was decomposed into the zero-loss (elastic) peak (ZLP) and the inelastic-loss spectrum, as shown in figure 5. Therefore, the heat power generated by the CEB is given by

$$Q = \frac{I_0}{q_e}\frac{S_p}{S_0}\int_0^{E_c} P(E)E\,\mathrm{d}E, \qquad \int_0^{E_c} P(E)\,\mathrm{d}E = 1, \quad (1)$$

where I_0 is the beam current in amperes, q_e is the electron charge, S_p and S_0 are the integrals of the inelastic-loss spectrum and the total EELS spectrum, respectively. $P(E)$ is the normalized inelastic-loss distribution, E is the energy loss and E_c is the cutoff energy of the inelastic loss. In the finite element thermal analysis, we use the heat generation rate to simulate the heating effect of the CEB. The heat generation rate is given by

$$Q' = \frac{Q}{\pi r^2 t}, \quad (2)$$

where r is the radius of the CEB, and t is the thickness of the specimen. In the present work, we take $E_c = 2000$ eV, $r = 1.5$ nm and $t = 50$ nm for the calculations. The beam current is measured as about 3.47 nA. Therefore, the heat generation rate calculated is about 3.0×10^{-10} W nm^{-3}. The EELS spectrum above 2000 eV is acquired insufficiently due to the weak signals, which can be estimated by the power-law

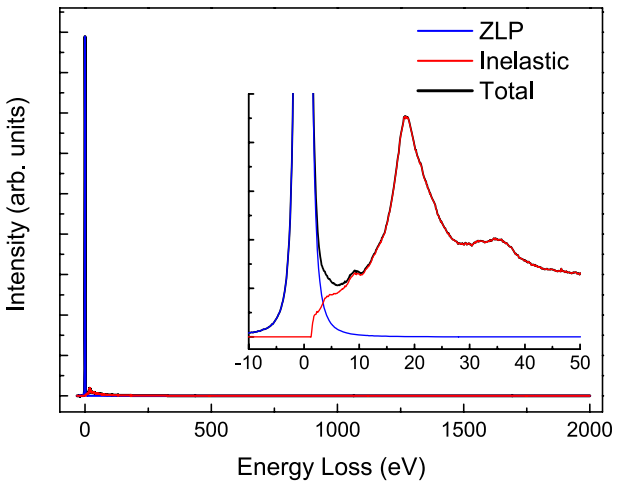

Figure 5. EELS spectrum of the ZnO membrane, which is decomposed into the zero-loss peak (red curve) and the inelastic-loss spectrum (blue curve). Magnified spectra are given in the inset.

extrapolation [23]. In this case, the influence of the EELS spectrum above 2000 eV on the result is smaller than 1%, which is negligible.

In the finite element thermal analysis, a ZnO disc was built with a radius of 1500 nm and a thickness of 50 nm. Considering the symmetry, the model can be simplified to a 45° sector. The schematic model is shown in figure 6(a). The heat was generated in a cylinder volume of 1.5 nm in radius at the centre of the ZnO disc. The temperature of the side surface of the ZnO disc was set to 20 °C as the boundary condition. When the thermal conductivity of bulk ZnO (60 W m^{-1} K^{-1}) is used, the temperature distribution is given in figure 6(b). The increased temperature is only about 0.04 °C. Considering the significant decrease of the thermal conductivity in nanomaterials [24–26], we decreased the thermal conductivity to 0.6 W m^{-1} K^{-1}. The increased temperature is about 4.2 °C, as shown in figure 6(c). According to the above results, we conclude that the heating effect of the CEB used is negligible in this work, and the sculpture of the CEB is predominated by the knock-on damage or ionization of the high-energy electrons. This conclusion is consistent with the finding of there being no distinct influence on the sculpture when the specimens were cooled to −88 °C.

4. Conclusions

In conclusion, we have demonstrated the fabrication of ultrafine nanostructures with single-nanometre precision in both feature size and location. The highly ordered ultrafine nanostructures, the ability to penetrate a diverse variety of solid-state materials, the extremity of sub-nanometre feature size and the large aspect-ratio up to 50 have been demonstrated in this work. Finite element thermal analysis has been attempted to qualitatively estimate the heating effect of the CEB according to the experimental results of EELS. The calculations reveal that the heating effect of the CEB is negligible in inorganic solid-state materials, and the sculpting of nanostructures is predominated by the knock-on damage or ionization of high-energy electrons. Our approach may be promising in the fabrication of nanodevices. For instance, liquids confined in nanopores are extremely interesting to study quantum fluidics; nanogratings comparable to particle wavelength are particularly interesting to study atomic wave diffraction, etc. The potential of this approach might be further enhanced by improvements on the commercialized TEM. Using a spherical aberration-corrected TEM, the current density will be increased by one order of magnitude, which can further increase the penetration ability and the speed of nanosculpture.

Acknowledgments

The authors thank Dr J Xiang (Department of Chemistry and Chemical Biology, Harvard University, Cambridge, Massachusetts) for the discussions of finite element thermal

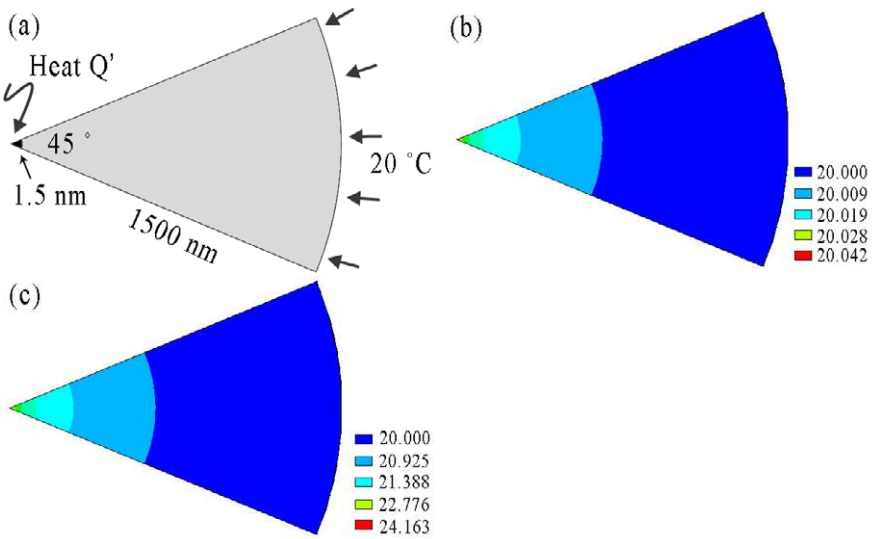

Figure 6. (a) Schematic model of a ZnO membrane for finite element thermal analysis. (b) Temperature distribution with a thermal conductivity of 60 W m^{-1} K^{-1}. (b) Temperature distribution with a thermal conductivity of 0.6 W m^{-1} K^{-1}.

analysis. This project is financially supported by the National Natural Science Foundation of China, and national 973 projects (No.2002CB613505, MOST). D P Yu is supported by the Cheung Kong Scholar Program, Ministry of Education, PR China, and a project from the Engineering Research Institute, Peking University.

References

[1] Ding G Q, Shen W Z, Zheng M J and Zhou Z B 2006 *Nanotechnology* **17** 2590
[2] Zeng A S, Zheng M J, Ma L and Shen W Z 2006 *Nanotechnology* **17** 4163
[3] Howorka S, Cheley S and Bayley H 2001 *Nat. Biotechnol.* **19** 636
[4] Li J L, Gershaw M, Stein D, Brandin E and Golovchenko J 2003 *Nat. Mater.* **2** 611
[5] Harrison S, Ledden B, Uplinger J, Thomas B, Mitsui T, McNabb D S, Golovchenko J and Li J L 2004 *Biophys. J.* **86** 480A
[6] Ho C, Heng J B, Timp R, Aksimentiev O, Schulten K, Shaw A, Sligar S, Twesten R, Wen J G and Timp G 2004 *Biophys. J.* **86** 481A
[7] Kasianowicz J J 2004 *Nat. Mater.* **3** 355
[8] Storm A J, Chen J H, Zandbergen H W and Dekker C 2005 *Phys. Rev.* E **71** 051903
[9] Bundschuh R and Gerland U 2005 *Phys. Rev. Lett.* **95** 208104
[10] Hao L, Macfarlane J C, Lam S, Foley C P, Josephs-Franks P and Gallop J C 2005 *IEEE Trans. Appl. Supercond.* **15** 514
[11] Taniguchi J 2005 *Phys. Rev. Lett.* **94** 065301
[12] Grisenti R E, Schollkopf W and Toennies J P 2000 *Phys. Rev.* A **61** 033608
[13] Cronin A D and Perreault J D 2004 *Phys. Rev.* A **70** 043607
[14] Perreault J D and Cronin A D 2005 *Phys. Rev.* A **71** 053612
[15] Li J L, Stein D, McMullan C, Branton D, Aziz M J and Golovchenko J 2001 *Nature* **12** 166
[16] Storm A J, Chen J H, Ling X S, Zandbergen H W and Dekker C 2003 *Nat. Mater.* **2** 537
[17] Kong Y C, Yu D P, Zhang B, Fang W and Feng S Q 2001 *Appl. Phys. Lett.* **78** 407
[18] Xu L F, Guo Y, Liao Q, Zhang J P and Xu D S 2005 *J. Phys. Chem.* B **109** 13519
[19] Zhao Q, Xu J, Xu X Y, Wang Z and Yu D P 2004 *Appl. Phys. Lett.* **85** 5331
[20] Zhang Y J, Wang N L, He R R, Zhang Q, Zhu J and Yan Y J 2000 *J. Mater. Res.* **15** 1048
[21] Williams D B and Carter C B 1996 *Transmission Electron Microscopy* (New York: Plenum)
[22] Hren J J, Goldstein J I and Joy D C 1979 *Introduction to Analytical Electron Microscopy* (New York: Plenum)
[23] Egerton R F 1996 *Electron Energy-Loss Spectroscopy in the Electron Microscope* 2nd edn (New York: Plenum)
[24] Lü X, Shen W Z and Chu J H 2002 *J. Appl. Phys.* **91** 1542
[25] Shi L, Hao Q, Yu C, Mingo N, Kong X Y and Wang Z L 2004 *Appl. Phys. Lett.* **84** 2638
[26] Yang R, Chen G and Dresselhaus M S 2005 *Phys. Rev.* B **72** 125418